J Mater Sci (2009) 44:4781–4788
DOI 10.1007/s10853-009-3720-4

Structure and properties of lead and lead sulfide nanoparticles in natural zeolite

J. F. Román-Zamorano · M. Flores-Acosta · H. Arizpe-Chávez · F. F. Castillón-Barraza · M. H. Farías · R. Ramírez-Bon

Received: 9 February 2009 / Accepted: 1 July 2009 / Published online: 23 July 2009

Abstract We have synthesized lead and lead sulfide nanoparticles embedded in a natural zeolite (clinoptilolite) matrix by a simple hydrothermal process. The process steps involve the partial removing of the natural cations in clinoptilolite, the ion-exchange process to enclose Pb ions and nanoparticles and finally a sulfuration process at different temperatures to obtain lead sulfide phases in the zeolite matrix. The samples were studied by X-ray diffraction, diffuse reflectance spectroscopy, energy dispersive X-ray spectroscopy, X-ray photon spectroscopy and transmission electron microscopy. The experimental results show the inclusion of three Pb species with different valence states after the Pb ion-exchange step, namely Pb^{2+}, Pb^{4+}, and Pb^{0}. At the end of the process, two simultaneous lead sulfide crystalline phases, PbS (Galena) and PbS_2 (tetragonal) were synthesized in the clinoptilolite matrix. The optical absorption spectra of the samples show the exciton absorption peaks typical of colloidal PbS nanoparticles. The average size of the PbS nanoparticles was about 10 nm and their crystalline structure was determined from diffraction electron patterns. The high-pressure phase PbS_2 was also identified and its formation was attributed to the influence of the special conditions of clinoptilolite matrix as crystallization media to induce some selective nucleation process of this crystalline phase.

J. F. Román-Zamorano · H. Arizpe-Chávez · R. Ramírez-Bon (✉)
Centro de Investigación y de Estudios Avanzados del I.P.N. Unidad Querétaro, Apdo. Postal 1-798, Querétaro, Qro 76001, México
e-mail: rrbon@qro.cinvestav.mx

M. Flores-Acosta · H. Arizpe-Chávez
Centro de Investigación en Física, Universidad de Sonora, Apdo. Postal 142, Hermosillo, Sonora 83190, México

F. F. Castillón-Barraza · M. H. Farías
Centro de Nanociencias y Nanotecnología, Universidad Nacional Autónoma de México, Apdo. Postal 2681, Ensenada 22800, B.C, México

Introduction

Zeolites are crystalline aluminosilicates whose framework consists of SiO_4 and AlO_4 tetrahedra joined by sharing oxygen atoms to form a highly regular three dimensional structure of cages and channels. The negative charges of AlO_4 units are compensated by the presence of exchangeable cations, mainly elements of groups IA and IIA. Perhaps the most commercially valuable and dynamic property of zeolites is their cation exchange capability. They also act as molecular sieves, because depending on the size and shape, some molecules can pass through, and others are either excluded or broken down by zeolites. Because of their unique porous properties and ion exchange capability, zeolites are extensively used in a variety of applications in petrochemicals, water purification, agriculture, animal husbandry, and construction. Nowadays most of zeolites employed in industry are synthetic, although natural zeolites are abundant in the earth surface. Clinoptilolite is one of the most abundant and widespread natural zeolite in the world. It is a high Si/Al ratio zeolite with high thermal stability, resistance against radiation and stable in a large range of pH. Being a naturally occurring mineral, the precise chemical composition of clinoptilolite is subject to a degree of variation depending on its origin region. However, approximate empirical formulas have been developed, being $(Ca, Fe, K, Mg, Na)_{3-6}Si_{30}Al_6O_{72}{\cdot}24H_2O$ a typical one. Clinoptilolite from several regions in the world have shown great capability

for heavy metal cations interchange including Pb^{2+}, Cd^{2+}, Zn^{2+}, Ni^{2+}, Ag^{+}, As^{3+}, etc., and radioactive isotopes of Cs^{+} and Sr^{2+} [1–5].

The porous structure and ion exchange capability properties of zeolites have been widely exploited to enclose a variety of materials in their nanometric cavities. In particular, semiconductor clusters enclosed in the zeolite cages following the same three dimensional array exhibit very interesting properties [6–9]. Most of the research has been done employing synthetic zeolites as templates, however, some recent papers have been focused on natural zeolites templates for the inclusion of diverse types of semiconductors [10–15]. The reduced size of the cavities is in many cases the upper limit for the semiconductor clusters size. In some other cases, depending on the availability of the precursor ions during the synthesis process, the cluster size can exceed the cavity dimensions. Even in these cases, the effect of the zeolite matrix on the growth of semiconductor clusters is important to stabilize their size at nanometric dimensions [16–18]. For this, it is very important to control the synthesis parameters. The reduction in the size of semiconductor particles to dimensions smaller than the exciton Bohr diameter yields to materials with size dependent of optical, electronic and chemical properties. In the case of the compound semiconductor PbS with a bulk energy bandgap of 0.41 eV [19] and a large exciton Bohr diameter of 18 nm [20], the strong confinement regime, as described by Efros and Efros [21], has been attained in nanoparticles hosted in several types of matrixes such as silicate glasses [22], conducting polymers [23–25], polyvinyl alcohol [26], 1-thioglycerol/dithioglycerol [27], and zeolites [6, 18, 28, 29]. We have also found that crystalline spherical-shaped PbS nanoparticles can be synthesized in zeolite Na-A and Na-X. The behavior of the crystalline PbS nanoparticles with cubic structure (Galena) in these matrix is very similar to that of colloidal PbS nanoparticles stabilized with polyvinyl alcohol (PVA) [26, 30], with size in the strong quantum confinement regime which is manifested through excitonic absorption bands in the absorption spectra at energies much higher than the energy band gap of bulk PbS.

In this study, we have explored the feasibility to employ clinoptilolite as the matrix to enclose PbS nanoparticles, taking advantage on its affinity to interchange Pb^{2+} cations. We investigated the properties of lead and lead sulfide nanoparticles which were stabilized in the natural zeolite clinoptilolite matrix by means of a hydrothermal process. We describe the synthesis process and the properties of the resulting samples. Pb nanoparticles embedded in the clinoptilolite matrix were obtained as an intermediate product of the process. Among the interesting features about the properties of the lead sulfide nanoparticles in the clinoptilolite are their crystalline structure and stoichiometry: it was determined that they coexist in two crystalline phases, PbS (Galena) and PbS_2 (tetragonal) structures.

Experimental details

We synthesized lead and lead sulfide nanoparticles into the clinoptilolite matrix, taking advantage on the cation exchange capability of this material, which can be described by the formula (NaKMgCaFe) $[(SiO_2)_{30}(AlO_2)_6]\cdot 2H_2O$. The amounts of the cations in the natural zeolite determined by energy dispersive X-ray spectroscopy (EDS) were 0.85, 1.86, 3.07, 1.37 and 1.62 wt% for Na, K, Mg, Ca, and Fe, respectively. This zeolite was obtained from a deposit in the state of Sonora in northern Mexico. The synthesis process was performed in three steps:

1. Removing of clinoptilolite cations: this step consisted in an exchange process of NH_4^{+} ions from an aqueous solution by the natural zeolite cations. Particularly, clinoptilolite is well known by its ability to exchange cation sites by NH_4^{+} ions from ammonia sources [31]. Whereas the NH_4^{+} ions decompose in NH_3 (gas) plus H^{+} ions which remain bonded to the active sites, replacing the removed cations. This ion exchange was accomplished by refluxing the zeolite in a 0.1 M solution of NH_4NO_3 for 3 h. After this time, the mixture was separated by filtration. Then the product was successively rinsed in deionised water, HCl solution (0.06 M), NaOH solution (0.06 M), and deionised water again. Finally, the material was vacuum dried at room temperature. From this first step we obtained clinoptilolite–H^{+} in powder form. After this process the chemical composition of the zeolite was determined from EDS again and the contents of cations were 0.83, 1.02, 0.12, 0.82, and 1.07 wt% for Na, K, Mg, Ca, and Fe, respectively. Although the natural cations in the natural zeolite were not completely removed, the total amount of cations was considerably reduced after this step.
2. Cation exchange: the H^{+} ions bonded within the zeolite structure can be removed either by dissociation in solution or by direct replacement with other positive ions. We used an aqueous lead solution to exchange H^{+} by Pb ions. For this purpose, 1 g of clinoptilolite–H^{+} powder was magnetically stirred in a 0.1 M solution of 20 mL of lead acetate, $Pb(CH_3OOH)_2$, at 50 ° C for 30 min. This product was extensively rinsed several times in deionised water. From this step we expected to obtain the product clinoptilolite–Pb.
3. Sulfuration: PbS was finally obtained by reaction of the product clinoptilolite–Pb in an aqueous sulfur source. One gram of clinoptilolite–Pb powder was

magnetically stirred in 40 mL of 0.1 M thiourea ($CS(NH_2)_2$) for 45 min. Three different samples were prepared at three different reaction temperatures: 20, 35 and 55 °C. Then, the samples were extensively rinsed and collected by filtration. They were powders with lackluster white color which presented no changes at ambient conditions. The crystalline structure of the samples was studied by X-ray diffraction (XRD) measurements performed in a Rigaku D/max-2100 diffractometer. Optical absorption spectra were obtained from diffuse reflectance spectroscopy measurements using the Kubelka–Munk theory. These measurements were obtained with a Perkin Elmer Lambda 19 spectrophotometer. The size of lead sulfur particles was determined from transmission electron microscopy (TEM) measurements made in a JEOL 2010 microscope. Also, X-ray photoelectron spectroscopy (XPS) measurements in a RIBER; CAMAC-3 spectrometer were done to investigate the valence-state of lead ions enclosed in the zeolite cavities prior to the sulfidation process and surface composition of Al, Si, O, and Pb of the studied samples.

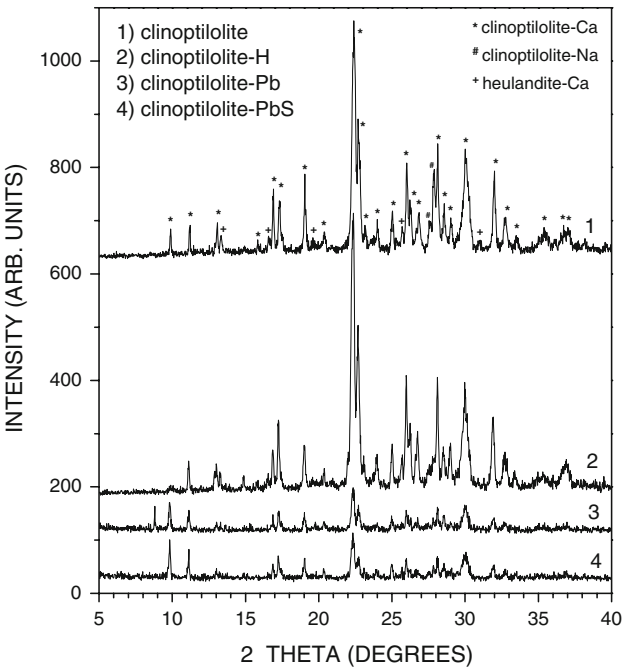

Fig. 1 XRD patterns of the clinoptilolite samples after each one of the steps of the synthesis process. At the bottom it is included the pattern of the unprocessed clinoptilolite

Results and discussion

The X-ray diffraction patterns of the clinoptilolite samples after each steps of the synthesis process are shown in Fig. 1. For comparison it was also included the pattern of the clinoptilolite sample previous to processing, where the diffraction peaks are labeled according to the corresponding crystalline phases identified in the sample. As can be seen, most of the peaks, including those with highest intensity, are related with the clinoptilolite–Ca crystalline phase (JCPDS # 039-1383). Some other peaks with lower intensity can be related with clinoptilolite–Na (JCPDS # 079-1461) and heulandite-Ca (JCPDS # 041-1357) phases. Thus, our natural zeolite clinoptilolite has some amount of huelandite which is frequently observed in natural zeolite tuffs. Since the XRD patterns of these two natural zeolites of the same family are quite similar, one of the criteria [32, 33] to identify them is by the intensity of the (020) and (004) diffraction peaks at about 10° and 22°, respectively; for clinoptilolite the (004) is the most intense peak in the pattern, which is our case, meanwhile, the (020) is the most intense diffraction peak observed in the pattern of heulandite. The pattern of the clinoptilolite–H sample after the first step of the synthesis process displays the same diffraction peaks than the clinoptilolite pattern with different peaks intensities associated mainly to differences in nature, amount and position of extraframework species in the clinoptilolite pores and channels [31, 34]. On the other hand, the patterns of the clinoptilolite samples loaded with Pb and PbS display most of the diffraction peaks of clinoptilolite with lower intensity. The clinoptilolite–PbS sample corresponds to that sulfurized at 50 °C. Neither Pb nor PbS diffraction peaks were observed in these patterns. In the case of clinoptilolite–Pb sample, this is because the amorphous nature of Pb enclosed in the zeolite as discussed below in the analysis of electron diffraction measurements and in the case of clinoptilolite–PbS sample because its PbS content is below the detection limit of XRD technique. The essential diffraction peaks displayed in the upper pattern (clinoptilolite sample) appear at the same positions as the diffraction peaks from the products of the different steps with different intensities, which as mentioned is consequence of the removing and reordering of the different cations species in the zeolite matrix and also due to the inclusion of Pb and PbS. Therefore, the basic clinoptilolite structure is not affected throughout the synthesis process.

Information about the chemical state of Pb ions within the zeolite network after the second synthesis step was provided by XPS measurements. In Fig. 2 it is shown the spectrum in the Pb 4*f* region for one clinoptilolite–Pb sample. The dotted line corresponds to the experimental data and the thick solid line is the best fit to three Gaussian peaks, whose deconvoluted plots are shown as thin solid lines in the graph. The electron binding energies corresponding to each band can be associated to the three lead

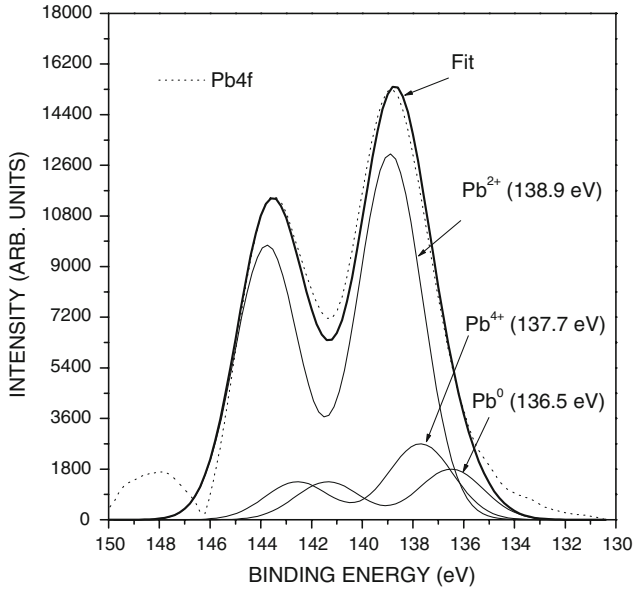

Fig. 2 XPS spectrum in the Pb 4*f* region for one clinoptilolite–Pb sample

valence states Pb^{2+} (138.9 eV), Pb^{4+} (137.7 eV) [35], and Pb^{0} (136.5 eV) in the form of lead nanoparticles in a close agreement with Liu et al. [36] in PtPb/C catalysts. Therefore, after the second step of the synthesis process, Pb species with stable valence sates of 0, +2 and +4 [37] were included in the clinoptilolite matrix. The intensity of the bands is related with the abundance of the Pb species in the sample, being the bands associated with Pb^{2+} ions the most intense ones. The presence of Pb^{4+} ions (which is thermodynamically less stable than Pb^{2+} ions) at 137.7 eV, could be explained by a partial re-oxidation process in the clinoptilolite surface due to the presence of OH^{-} groups in order to form $Pb(OH)_4$ species. Interesting is the presence of neutral Pb^{0} as metallic nanoparticles evidencing the precipitation of metallic Pb in the clinoptilolite matrix, which was addressed by TEM images measurements, as shown below. The elemental analysis of the clinoptilolite–Pb sample was also performed from XPS measurements. This analysis was done by using a method proposed by Soto et al. [38]. The result shows that the amount of Pb in this sample is 10 wt%.

In Fig. 3 it is shown the image of a clinoptilolite crystal with embedded nanometric-sized Pb particles. Spherical-shaped nanoparticles are observed on the surface of clinoptilolite crystal with an average size of about 5 nm. The diffraction electron measurements to determine the crystalline structure of the observed nanoparticles did not show any crystalline pattern, which indicated their amorphous nature. Furthermore, the precipitation of Pb^{0} nanoparticles in the clinoptilolite matrix was also inferred from the absorption spectrum of the clinoptilolite–Pb sample, shown as dotted line in Fig. 4. An intense broad absorption band is observed in the UV region centered at about 213 nm. In addition, a clear shoulder appears at about 230 nm and

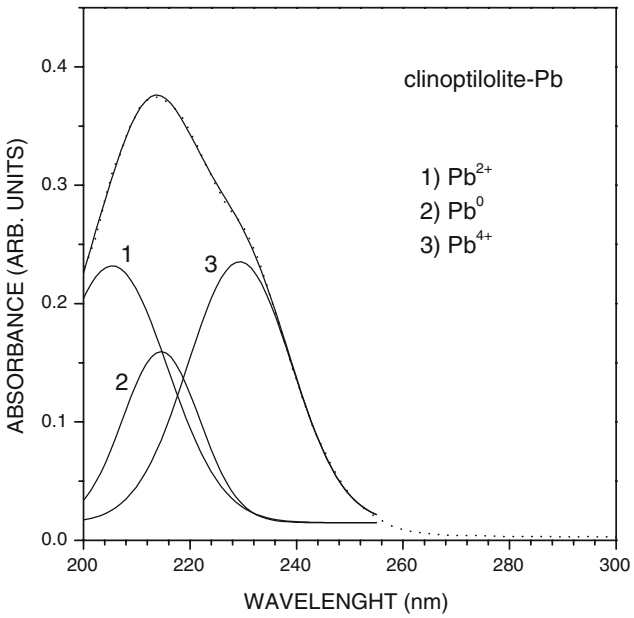

Fig. 4 Absorption spectra of the clinoptilolite–Pb sample

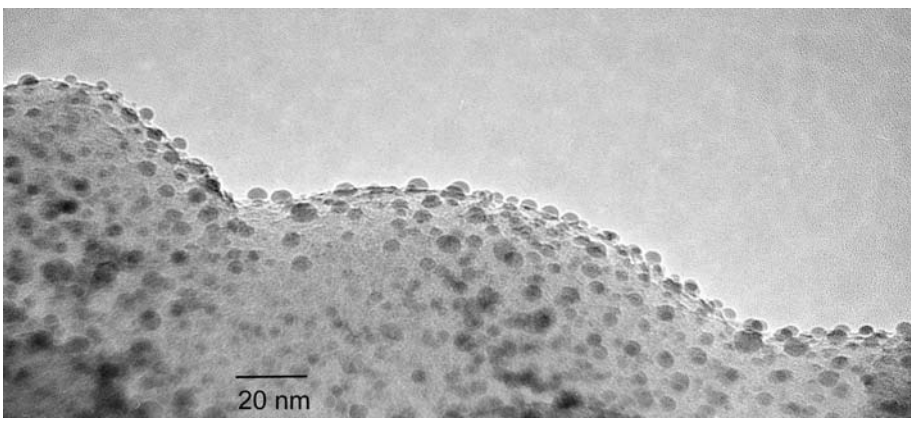

Fig. 3 TEM image of a clinoptilolite crystal with embedded Pb nanoparticles

other less evident peak is located at about 205 nm. Since all the absorption spectra were measured taking as reference the clinoptilolite–H sample, it can be inferred that the absorption features in Fig. 4 are completely produced by the Pb species included in the sample after the Pb exchanging process. The experimental absorption spectrum was fitted to three Gaussian peaks represented by the solid line which lies upon the dotted one. Each one of the Gaussian peaks contributing to the wide absorption signal, centered at about 205, 214 and 230 nm, respectively, are also plotted in this graph. The absorption band at about 205 nm can be assigned to the absorption of Pb^{2+} ions. A very similar absorption band centered at 207 nm has been observed for Pb^{2+} ions in solutions of $Pb(ClO_4)_2$ containing 2-propanol and (poly)ethyleneimine (PEI) as polymer stabilizer [39]. Furthermore, the reduction of Pb^{2+} ions by γ irradiation in these solutions produced stable Pb colloidal nanoparticles with size about 10 nm which originate an absorption band at 218 nm, related with surface plasmon oscillations in the Pb nanoparticles. The wavelength at which this band appears in this spectrum is very close to the one expected for surface plasmon in lead and it has also been observed in other reports [40, 41]. Therefore, in our case, the absorption band at about 214 nm can be assigned to surface plasmon oscillations in Pb nanoparticles in the clinoptilolite matrix. These results show that the behavior of Pb^{2+} ions and Pb nanoparticles in the clinoptilolite matrix is similar to that of colloidal species stabilized in solutions. The TEM image of the Pb nanoparticles in the clinoptilolite matrix (Fig. 3) resembles colloidal particles in solution. Taking into account that Pb^{4+} ions are also present in the clinoptilolite matrix, the origin of the absorption band at 230 nm could be associated to the optical absorption by these ions. There is not much information about the optical absorption of Pb^{4+} ions in literature. Thus, the information provided by optical absorption spectroscopy about clinoptilolite–Pb samples would be quite consistent with the above XPS analysis.

In Fig. 5, are plotted the optical absorption spectra of the lead sulfide loaded clinoptilolite samples obtained at three different sulfidation temperatures, namely, 25, 35 and 55 °C. In this graph, the spectrum of the clinoptilolite–Pb sample was also included for comparison purposes. It does not show any absorption feature in the visible range. On the other hand, the spectra of the clinoptilolite–PbS samples display two broad absorption bands centered at about 600 and 400 nm. The intensity of the absorption bands increases with the sulfidation temperature, indicating a larger precipitation of lead sulfide into these samples. Although the absorption bands are quite broad, they can be related with the excitonic transitions like the ones observed in the optical absorption spectra of PbS colloidal nanoparticles in solution [42–45], polymers [23], Langmuir–Blodget monolayers

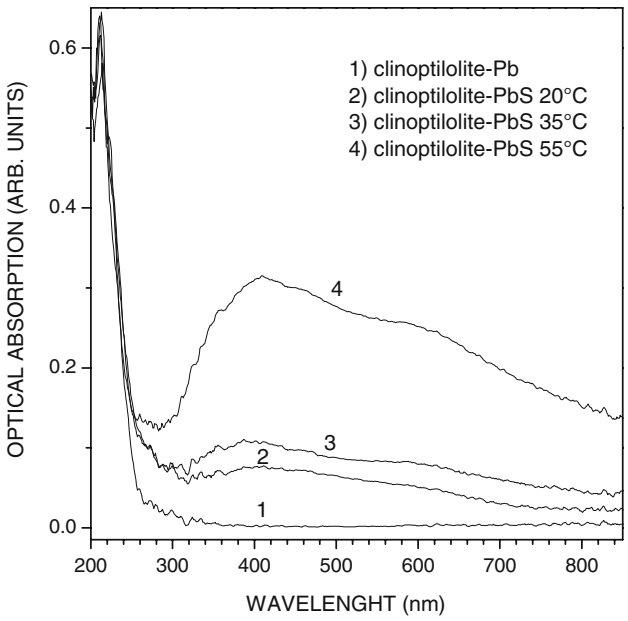

Fig. 5 Optical absorption spectra of the lead sulfide loaded clinoptilolite samples obtained at 25, 35 and 55 °C sulfidation temperatures

[46], zeolite A [18], and zeolite X [47]. The spectra of the clinoptilolite–PbS samples also display the surface plasmon absorption band located at 214 nm and already attributed to Pb nanoparticles in the spectrum of Fig. 4, indicating the presence of unsulfurized Pb in the clinoptilolite matrix for these samples.

The size and shape of the lead sulfide nanoparticles in the clinoptilolite matrix can be observed in the TEM image shown in Fig. 6. The image displays the edge of a clinoptilolite crystallite where uniformly embedded nanometric-sized particles with roughly round shape can be observed. However, flat faces in some of these nanoparticles can be noticed. The size distribution of the nanoparticles obtained from TEM images is shown by the histogram in Fig. 7. The average size of the nanoparticles in this image is about 10 nm. The crystalline structure of the nanoparticles was

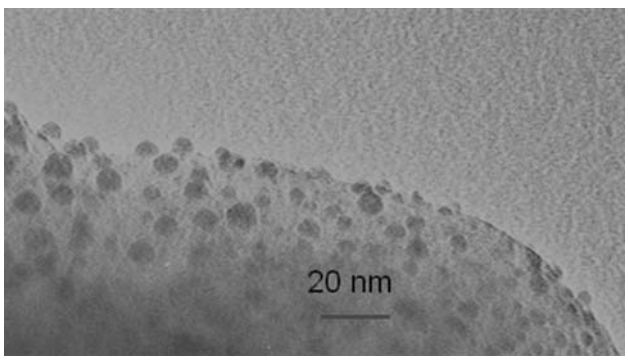

Fig. 6 TEM image of lead sulfide nanoparticles in the clinoptilolite matrix

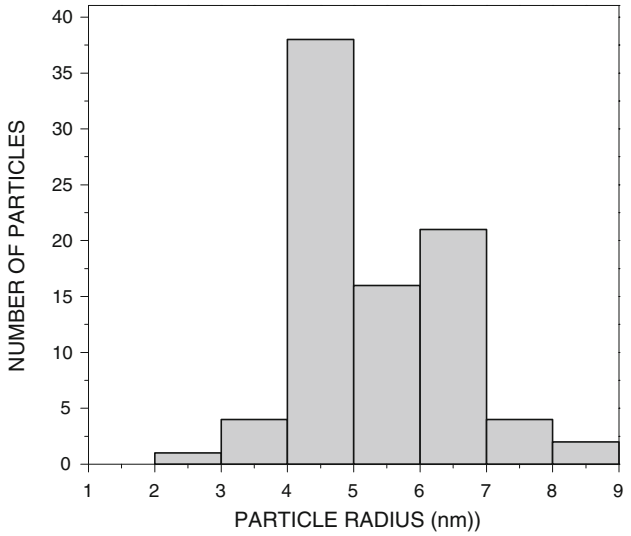

Fig. 7 Size distribution of the nanoparticles obtained from TEM images. The average size of the nanoparticles calculated from this histogram was 10.2 nm

determined from their electron diffraction (ED) patterns, shown in Fig. 8a, b for two different nanoparticles in the clinoptilolite matrix. The bright spots in these figures indicate their crystalline nature and provide an estimation of the interplanar distances in the crystalline lattices. The interplanar distances determined from these patterns are shown in Table 1 along with those corresponding to the cubic PbS (galena) (JCPDS # 050592) and tetragonal β-PbS_2 (JCPDS # 200596) phases and their corresponding crystalline planes. It can be seen that the pattern in Fig. 8a matches well with the cubic PbS crystalline phase, meanwhile that in Fig. 8b matches better with the tetragonal β-PbS_2 one. The numbers in the spots indicate the crystalline planes of each phase, according to the sequence in Table 1. Thus, in contrast with PbS nanoparticles with cubic crystalline structure synthesized in similar conditions in zeolites A-type and X-type, the nanoparticles embedded in this clinoptilolite matrix correspond to both phases, cubic PbS and the so called β-PbS_2 phase with tetragonal structure. Both, α- (hexagonal) and β-PbS_2 phases are considered high pressure phases because they are formed at pressures higher than 20 Kbar and temperatures above 600 °C [48], and to our knowledge, no reports exist for PbS_2 synthesized at atmospheric pressure [49]. However, there are reports on the formation of compressed PbS and α-PbS_2 phases in a matrix of poly-(ethylene oxide) (PEO) films at normal conditions (room temperature, 1 atm of pressure). The synthesis of these novel phases of lead sulfide was based on the employment of an appropriated polymer matrix to approach (mimic) the growth mechanisms in biological matrices, which are capable to synthesize some high-pressure metastable inorganic phases. The explanation to the

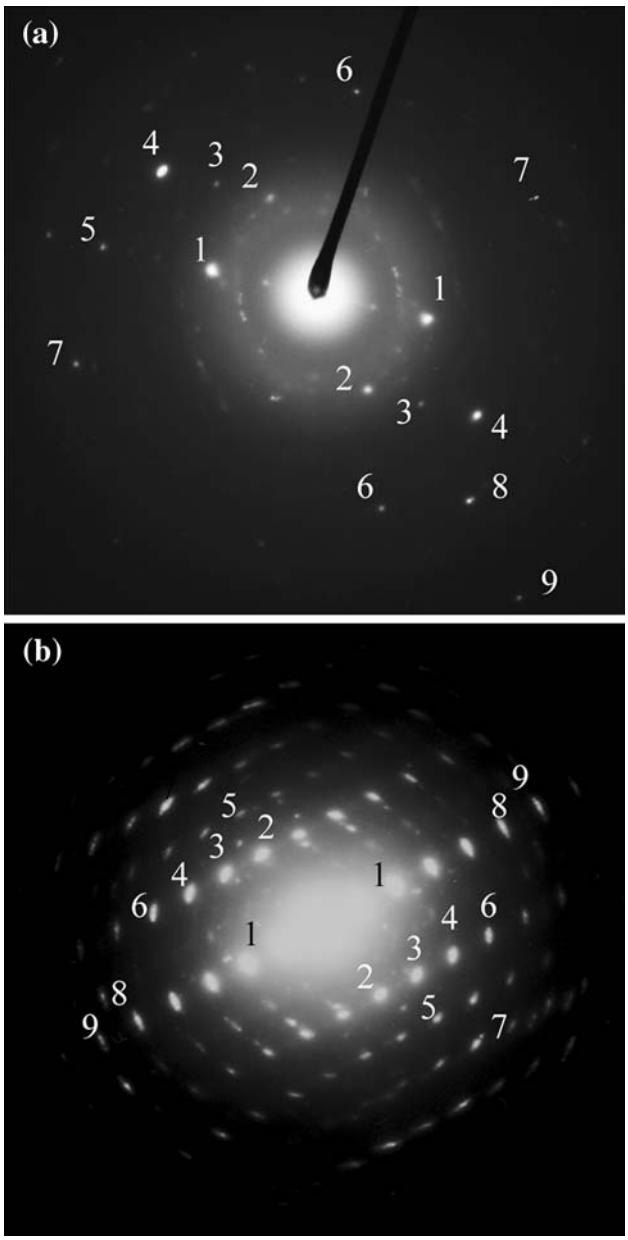

Fig. 8 ED patterns taken from two different nanoparticles in the clinoptilolite matrix: **a** pattern of PbS nanopartice and **b** pattern of PbS_2 nanoparticle

formation of these lead sulfide phases was not the conversion of galena PbS by high pressure exerted by the polymeric matrix but a selective nucleation of the compressed lead sulfide phases within specific places in the polymer. This nucleation is produced by the special properties of the polymer as a crystallization media, namely, its relative order, density, and rigidity. In our case, the properties of the clinoptilolite matrix fulfill the conditions observed in the polymeric matrix to induce the nucleation of compressed lead sulfide phases. In fact, in terms of these properties, zeolites with their rigid structure constituted by a high

Table 1 Interplanar distances corresponding to the cubic PbS (galena) (JCPDS # 050592) and tetragonal β-PbS_2 (JCPDS # 200596) phases and their corresponding crystalline planes

Interplanar distance (Å)		Interplanar distance (Å)		Crystalline planes	
Fig. 8a	Fig. 8b	c-PbS	β-PbS_2	c-PbS	β-PbS_2
3.34	3.54	3.42	3.73	(111)	(111)
3.01	3.01	2.96	3.07	(200)	(200)
2.15	2.73	2.09	2.83	(220)	(112)
1.77	2.23	1.79	2.17	(222)	(113)
1.72	1.94	1.71	1.93	(440)	(203)
1.36	1.77	1.36	1.87	(331)	(004)
1.30	1.58	1.32	1.60	(420)	(204)
1.25	1.36	1.21	1.36	(422)	(420)
0.97	1.16	0.98	1.20	(600)	(116)

regular array of pores and channels are much better than polymers. Therefore, we could expect a similar origin in the formation of the β-PbS_2 phase crystallized into the clinoptilolite matrix. Moreover, as discussed above, previous to sulfidation, clinoptilolite already contained Pb^{4+} ions which have the appropriate valence state to form the PbS_2 phase. Compared to PbS_2 particles stabilized in PEO films, the average size of the lead sulfide nanoparticles embedded in the clinoptilolite matrix is much smaller. This also accounts for the formation of the PbS_2 phase in the clinoptilolite matrix because some pressure phases are more common in nanocrystals than in bulk materials, due in part, to kinetic constraints imposed by the strong binding conditions in the size reduced systems. Thus, we conclude that clinoptilolite matrix can stabilize nanoparticles of both cubic PbS and tetragonal β-PbS_2 crystalline phases.

Conclusions

In this study we have reported the hydrothermal synthesis of two simultaneous lead sulfides crystalline phases corresponding to Galena PbS and tetragonal β-PbS_2 embedded in clinoptilolite matrix. Pb nanoparticles were also obtained as an intermediate product of the synthesis process, some of which remained after the sulfidation step. The lead sulfide crystalline nanoparticles with average size of about 10 nm behave like colloidal particles in solution. Broad excitonic bands observed in the absorption spectra of the lead sulfide nanoparticles show that their reduced size produces strong quantum confinement effects. The special properties of the clinoptilolite matrix as a crystallization media, account for the formation at low pressure of nanoparticles with PbS_2 crystalline phase. Clinoptilolite is an appropriated crystalline matrix to stabilize semiconductor particles at nanometric size, such as the ones reported here.

Acknowledgements We thank the technical assistance of Jesús Antonio Díaz, J. E. Urbina, M. A. Hernández L. and E. Larios. F:F. Castillón-Barraza also acknowledges to CONACyT and DGAPA-UNAM for research grants 50547 and IN110208-3, respectively.

References

1. Faghihian H, Ghannadi Marageh M, Kazemian H (1999) Appl Radiat Isot 50:660
2. Mondale KD, Carland RM, Aplan FF (1995) Min Eng 8:535
3. Cerjan Stefanovic S, Zabukovec Logar N, Margeta K, Novak Tusar N, Arcon I, Maver K, Kovac J, Kaucic V (2007) Microporous Mesoporous Mater 105:251
4. Dávila-Jiménez MM, Elizalde-González MP, Mattusch J, Morgenstern P, Pérez-Cruz MA, Reyes-Ortega Y, Wennrich R, Yee-Madeira H (2008) J Colloid Interface Sci 322:527
5. Erdem E, Karanipar N, Donat R (2004) J Colloid Interface Sci 280:309
6. Wang Y, Herron N (1987) J Phys Chem 91:257
7. Chen W, Wang ZG, Lin ZJ, Lin LY (1996) Solid State Commun 101:371
8. Herron N (1995) J Incl Phenom Macrocycl Chem 21:283
9. Suzuki S, Ryo M, Yamamoto T, Sakata T, Yanagida S, Wada Y (2007) J Mater Sci 42:5995. doi:10.1007/s10853-006-1127-z
10. Kadlecikova M, Breza J, Jesena K, Pastorkova K, Luptakova V, Kolmacka M, Vojackova A, Michalka M, Vavra I, Krizanova Z (2008) Appl Surf Sci 254:5073
11. Li F, Suna S, Jiang Y, Xia M, Suna M, Xue B (2008) J Hazard Mater 152:1037
12. Sohrabnezhad S, Pourahmad A, Sadjadi MS, Zanjanchi MA (2008) Mater Sci Eng C 28:202
13. Sadjadi MS, Pourahmad A, Sohrabnezhad S, Zare K (2007) Mater Lett 61:2923
14. Iacomi F, Vasile A, Polychroniadis EK (2003) Mater Sci Eng B 101:275
15. Martín-Palma RJ, Hernández-Vélez M, Díaz I, Villavicencio-García H, García-Poza MM, Martínez-Duart JM, Pérez-Pariente J (2001) Mater Sci Eng C 15:163
16. Sotelo-Lerma M, Quevedo-López MA, Orozco-Terán RA, Ramírez-Bon R, Espinoza-Beltrán FJ (1998) J Phys Chem Solids 59:145
17. Ochoa-Landín R, Flores-Acosta M, Ramírez-Bon R, Arizpe-Chávez H, Sotelo-Lerma M, Castillón-Barraza FF (2003) J Phys Chem Solids 64:2245
18. Flores-Acosta M, Sotelo-Lerma M, Arizpe-Chávez H, Castillón-Barraza FF, Ramírez-Bon R (2003) Solid State Commun 136:567
19. Xie R, Li D, Yang D, Jiang M (2007) J Mater Sci 42:1376. doi:10.1007/s10853-006-1211-4
20. Wise FW (2000) Acc Chem Res 33:773
21. Efros AIL, Efros AL (1982) Fiz Tekh Poluprov 16:1209
22. Espiau R, Bernas H (2005) J Appl Phys 98:104310
23. Wang Y, Suna A, Mahler W, Kasowski R (1987) J Chem Phys 87:7315
24. Asunskis DJ, Boloti IL, Hanley L (2008) J Phys Chem C 112:9555
25. Zhang Y, Xu Z (2008) Appl Phys Lett 93:083106
26. Kraus TD, Wise FW (1997) Phys Rev B 55:9860
27. Zhao X-S, Xu S-Y, Liang L-Y, Li T, Cauchi S (2007) J Mater Sci 42:4265. doi:10.1007/s10853-006-0679-2
28. Chen W, Wang Z, Lin Z, Qian J, Lin L (1990) Appl Phys Lett 68:91998
29. Leiggener C, Calzaferri G (2005) Chem A Eur J 11:7191
30. Kostic R, Romcevic M, Romcevic N, Klopotowski L, Kossut J, Kuljanin J, Comor MI, Nedeljkovic JM (2008) Opt Mater 30:1177

31. Rodríguez-Iznaga I, Gómez A, Rodríguez-Fuentes G, Benítez-Aguilar A, Serrano-Bayan J (2002) Microporous Mesoporous Mater 53:71
32. Perraki T, Orfanoudaki A (2004) Appl Clay Sci 25:9
33. Elaiopoulos K, Perraki Th, Grigoropoulou E (2008) Microporous Mesoporous Mater 112:441
34. Lee Y, Carr SW, Parised J (1998) Chem Mater 10:2561
35. Fuggle JC, Martensson N (1980) J Electron Spectrosc Relat Phenom 21:275
36. Liu Z, Guo B, Tay SW, Hong L, Zhang X (2008) J Power Sources 184:16
37. Ganguly P, Hedge MS (1988) Phys Rev B 37:5107
38. Soto G, Díaz JA, Machorro R, Reyes-Serrato A, de la Cruz W (2002) Mater Lett 52:29
39. Henglein A (1999) J Phys Chem B 103:9302
40. Henglein A, Holzwarth A, Mulvaney P (1992) J Phys Chem 96:8700
41. Mulvaney P (1996) Langmuir 12:788
42. Fernee MJ, Watt A, Warner J, Heckenberg N, Rubinsztein-Dunlop H (2004) Nanotech 15:1328
43. Fernee MJ, Watt A, Warner J, Cooper S, Heckenberg N, Rubinsztein-Dunlop H (2003) Nanotech 14:991
44. Cademartiri L, Montanari E, Calestani G, Migliori A, Guagliardi A, Ozin GA (2006) J Am Chem Soc 128:10337
45. Peterson JJ, Krauss TD (2006) Phys Chem Chem Phys 8:3851
46. Song Li L, Qu L, Wang L, Lu R, Peng X, Zhao Y, Li T (1997) Langmuir 13:6183
47. Flores-Acosta M, Pérez-Salas R, Sotelo-Lerma M, Castillón-Barraza FF, Ramírez-Bon R (2005) Adv Tech Mater Mater Process J 7:101
48. Pitcher MW, Cates E, Raboin L, Bianconi PA (2000) Chem Mater 12:1738
49. Wheeler KT, Walker D, Johnson MC (2007) Am J Sci 307:590